

Design of a Three-Axis Micro-scale Metrology System for the Characterization of  
Cylindrical Flexures

by

Ron M. Perez

SUBMITTED TO THE DEPARTMENT OF MECHANICAL ENGINEERING IN PARTIAL  
FULFILLMENT OF THE REQUIREMENTS FOR THE DEGREE OF

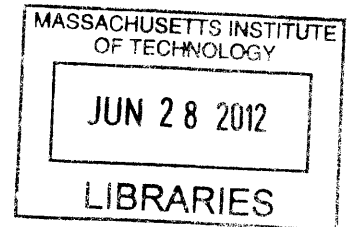
BACHELOR OF SCIENCE IN MECHANICAL ENGINEERING  
AT THE  
MASSACHUSETTS INSTITUTE OF TECHNOLOGY

JUNE 2012

©2012 Ron M. Perez. All rights reserved.

The author hereby grants to MIT permission to reproduce  
and to distribute publicly paper and electronic  
copies of this thesis document in whole or in part  
in any medium now known or hereafter created.

**ARCHIVES**



Signature of Author: \_\_\_\_\_

Department of Mechanical Engineering  
May 18, 2012

Certified by: \_\_\_\_\_

Martin L. Culpepper  
Associate Professor of Mechanical Engineering  
Thesis Supervisor

Accepted by: \_\_\_\_\_

Professor J. Lienhard V  
Samuel C. Collins Professor of Mechanical Engineering  
Undergraduate Officer



# Design of a Three-Axis Micro-scale Metrology System for the Characterization of Cylindrical Flexures

by

Ron M. Perez

Submitted to the Department of Mechanical Engineering  
on May 18, 2012 in Partial Fulfillment of the  
Requirements for the Degree of Bachelor of Science in  
Mechanical Engineering

## **ABSTRACT**

The objective of this thesis was to develop a laser metrology system in order to measure the movement in two of the rotation axes of a cylindrical flexure. The building and characterization of this system was achieved in an effort to measure cylindrical flexures such that rules for modeling them might be developed. The system developed measures translations of the flexure normal to the circular surface of the cylinder as well as rotations about the axes within this plane. While numerous metrology systems capable of achieving these functionalities exist, this system has inherent benefits in cost, range, and resolution. Using three lasers reflected off of mirrors mounted on a cylindrical flexure and captured by photodiodes, we are able to characterize micro-scale movements of the system with a resolution of 134  $\mu\text{m}$  and a range of 5.04cm of translation.

Thesis Supervisor: Martin L. Culpepper  
Title: Associate Professor of Mechanical Engineering



## **Acknowledgments**

This thesis was written by the grace of God extended abundantly to me through the help, encouragement and prayers of many people. Some of those people I'd like to highlight are:

Maria Telleria and Bob Panas – I've learned incredible amounts just writing this paper, and I would not have known where to start nor finish without you both. I cannot even begin to thank you for all your help and patience.

My parents, Ronald and Gloria – After a lifetime of push and love, it's needless to say that I would not be here without you both.

Mark – Thank you for encouraging me and helping me debug my circuit, even until 2:30 AM.

Zac – After 4 awesome years, you're still there still for me in a pinch. I hope to be able to do the same for you.

Dani, Laura, Wes, Kwami, Emily, Anders, Chris, and the rest of my brothers, sisters and friends – Your encouragement and prayers are greatly valued and appreciated by me, and I have no doubt that I could not have finished without them.

Jesus – I hope this makes it to your fridge! You never cease to amaze me.



## Table of Contents

<b>Abstract</b>	3
<b>Acknowledgements</b>	5
<b>Table of Contents</b>	7
<b>List of Figures</b>	8
<b>List of Tables</b>	9
<b>1. Introduction</b>	10
1.1 Background	12
1.1.1 Metrology Systems	12
1.1.1.1 Laser Interferometers	12
1.1.1.2 Coordinate Measuring Machine	13
1.1.1.3 Capacitance Probes	13
1.1.1.4 Linear Variable Differential Transformers	14
1.1.2 Cylindrical Flexures	14
<b>2. Single-Axis Design of Measurement System</b>	16
2.1 Signal Layout	16
2.2 Components	18
2.2.1 Laser	18
2.2.2 Quadrant Photodiode	18
2.2.3 Voltage Regulator	19
2.2.4 Operational Amplifier	20
<b>3. Calibration of Measurement System</b>	22
3.1 Calibration Setup	22
3.2 LabVIEW Program	23
3.3 System Noise	24
3.4 Calibration Results – Photodiode Resolution	26
<b>4. Multiple-Axis Design of Measurement System</b>	22
4.1 Flexure Stands	28
4.1.1 Laser Stand	28
4.1.1.1 Design Iteration 1	28
4.1.1.2 Design Iteration 2	30
4.1.2 Photodiode Flexure Stand	32
4.2 Angle Functions – Parameter Relations	35
4.2.1 Translations of Stage	35
4.2.2 Rotations of Stage	37
4.2.3 Multiple-Axis Rotations	39
4.2.4 Mirror Mounting	40
4.3 Range and Resolution	41
<b>5. Conclusion</b>	43
5.1 Overview	43
5.2 Future Work	43
<b>6. Appendices</b>	45
<b>Appendix A: Data Sheets</b>	45
<b>Appendix B: Technical Drawings</b>	48
<b>Appendix C: LabVIEW Code</b>	54
<b>7. References</b>	57

## List of Figures

<b>Figure 1-1:</b> An example of the setup of the final metrology system.	11
<b>Figure 1-2:</b> An example of a cylindrical flexure system	15
<b>Figure 1-3:</b> Diagrams of a loaded cylindrical flexure	15
<b>Figure 2-1:</b> Diagram of signal transfer	17
<b>Figure 2-2:</b> Photodiode output summation diagram	19
<b>Figure 2-3:</b> Diagram of the voltage regulator circuit used to supply constant voltage	20
<b>Figure 2-4:</b> Diagram of non-inverting operational amplifier circuit	21
<b>Figure 2-5:</b> Layout of operational amplifiers within LM324 chip	21
<b>Figure 3-1:</b> A picture of the original single axis setup	23
<b>Figure 3-2:</b> A plot of the noise from the DAQ board	24
<b>Figure 3-3:</b> A calibration plot	26
<b>Figure 4-1:</b> Solid model original single-part design of the laser stand flexure,	29
<b>Figure 4-2:</b> A profile view of a rectangular notch hinge	29
<b>Figure 4-3:</b> Redesign of the laser stand flexure	31
<b>Figure 4-4:</b> A profile view of the flexure found in the laser stand second design iteration	31
<b>Figure 4-5:</b> A solid model of the flexure stand assembly for the quadrant photodiode	33
<b>Figure 4-6:</b> A profile view of the flexure found in the photodiode stand flexures	33
<b>Figure 4-7:</b> An image of the assembled flexure stands	34
<b>Figure 4-8:</b> A modeling of the effect of the translation of the mirror on the reflected laser beam	36
<b>Figure 4-9:</b> A close-up angle study of the effect of rotations	39



## **List of Tables**

<b>TABLE 1-1:</b> A cost-performance chart of different metrology systems	<b>14</b>
<b>TABLE 4-1:</b> The properties of 6061 T6 Aluminum and the first design iteration of the rectangular notch hinge	<b>30</b>
<b>TABLE 4-2:</b> The properties of 1095 Spring Steel and the second design iteration of the rectangular notch hinge	<b>32</b>
<b>TABLE 5 -1:</b> Cost-performance summary of designed metrology system	<b>43</b>

## **1. Introduction**

The objective of this thesis was to develop a laser metrology system in order to measure the movement in two of the rotation axes of a cylindrical flexure. The building and characterization of this system was achieved in an effort to measure cylindrical flexures such that rules for modeling them might be developed, though it can be used to measure other moving parts that require high precision. The system developed measures translations of the flexure normal to the circular surface of the cylinder as well as rotations about the axes within this plane. While numerous metrology systems capable of achieving these functionalities exist, this system has inherent benefits in cost, range, and resolution. Using three lasers reflected off of mirrors mounted on a cylindrical flexure and captured by photodiodes, we are able to characterize micro-scale movements of the system with a resolution of 134  $\mu\text{m}$  and a range of 5.04cm of translation, with a system noise of 90 mV. Both the lasers and photodiodes are housed in flexure stands, enabling precise calibration of the laser on the surface of the photodiode. Shown in this paper are geometric, electrical, and mechanical characteristics of this system.

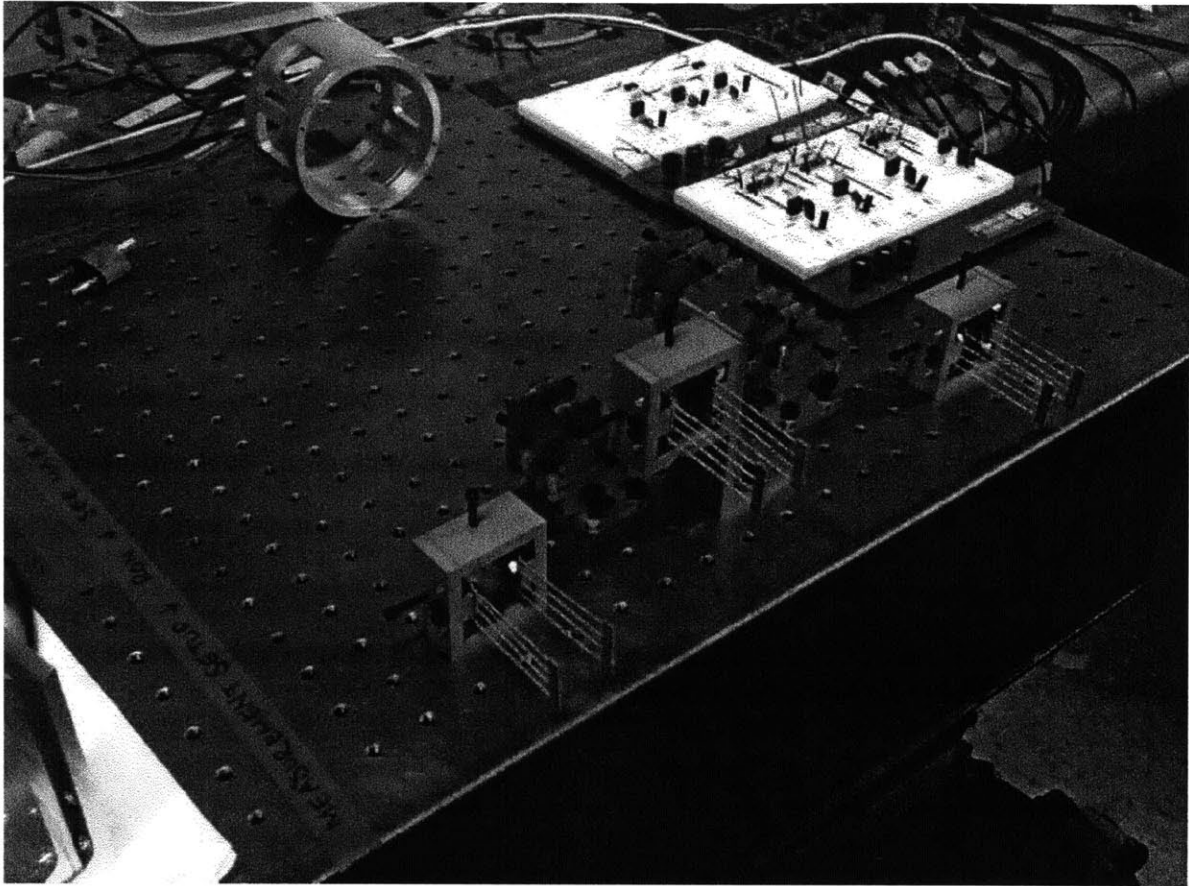


**Figure 1-1:** An example of the setup of the final metrology system.

## ***1.1 Background***

It is important to characterize precision systems such as these because of their use in measuring the performance of flexure systems. We want to be able to use this system to take measurements in multiple degrees of freedom so we can know how the cylindrical flexure will respond given a certain input. Aside from demonstrating their capabilities, this data is useful in the optimization of flexure systems as well as identifying areas of error or problems in manufacturing or performance. Quantifying these things enables us to test new ideas and solutions. In order to characterize flexure systems such as cylindrical flexures, it is important for our metrology system to have an appropriate range and resolution. In this case, it is ideal to have a high resolution—on a micro-scale—and a fairly large range—on the order of several centimeters.

### ***1.1.1 Metrology Systems***

There are numerous metrology systems of various sizes and applications in existence, which are briefly covered in the paragraphs below. For this project we have chosen to expand on a method implemented by Ryan King that uses lasers aimed at mirrors positioned on the flexure reflected onto quadrant photodiodes [1]. This method was chosen for its advantages in cost, range, and resolution over existing measurement systems, which include:

#### ***1.1.1.1 Laser Interferometers***

This is one form of six-axis metrology system that provides accurate measurements by interfering two beams of light and observing changes in their interference pattern. By reflecting a measurement beam off of a reflecting surface on the target, the relative phase of the measurement beam and a static reference beam changes. Changes in relative phase of the two beams result in constructive or destructive interference that can be detected by changes in the fringe pattern of the recombined beam. While basic interferometers have a measurement

resolution of around 0.32  $\mu\text{m}$ , improvements in resolution can be achieved through multiple passes that increase the optical path length and amplify the displacement of the target mirror, as well as through interpolation of the fringe patterns and through use of the beat frequency generated by recombining beams with different frequencies. However, these measures can be costly and hard to fit into small spaces. This is because each measurement axis requires a separate interferometer and receiver, as well as the amount of expensive components involved in measuring multiple axes at a desired resolution.

#### *1.1.1.2 Coordinate Measuring Machine*

A CMM is a machine that moves a touch probe in three orthogonal directions to measure size, position, or displacement in 3-dimensional space. Mostly intended for comparing fabricated parts to their theoretical designs, CMM's are often fairly large in size, taking up the space of a large granite table with guide rails and a bridge on with the head of the machine is mounted. While this method of measurement is versatile, it is ill-suited to taking measurements of a dynamic and relatively small system such as ours.

#### *1.1.1.3 Capacitance Probes*

This method of measurement involves using capacitors mounting a probe near or on the surface of a part and measuring the capacitance between the two surfaces, characterized by  $C = \frac{\epsilon A}{d}$ , where  $\epsilon$  is the dielectric constant of the medium between the two surfaces. While this method is relatively inexpensive and can be integrated into smaller systems, its largest drawback is the limited range. Because they must be mounted for capacitance, generally anything over 100  $\mu\text{m}$  is outside the range. In measuring CF's, we hope to achieve a range of at least 1 mm.

#### 1.1.1.4 Linear Variable Differential Transformers

LVDT's measure linear displacement using a transformer that consists of three solenoidal coils surrounding a ferromagnetic core. The center coil is driven by an alternating current, and the core is attached to the part that one is measuring. As the core is slid along the axis of a tube by the moving part it is attached to, it induces a voltage in either of the secondary coils as it passes through it. This voltage is proportional to the length of the core that has passed through the secondary coil, as characterized by the Maxwell-Faraday equation. While LVDT's can be arranged such that they could measure multiple axes, using multiple transformers for this purpose can get relatively expensive.

Though various systems for linear and rotational motion measuring exist, our system holds inherent advantages for our purposes.

**TABLE 1-1:** A cost-performance chart of different metrology systems.

	Highest Resolution Available (nm)	Price (\$1000's)	Range	Size
Interferometer	1	10-100	1 m	1 x 1 m atop optical table
CMM	100	100-200	1 m <sup>3</sup>	2 x 2 x 2 m machine w/granite table
Capacitance Probes	10	1-10 per probe	100 μm	1 cm length cylinder w/ 0.5 cm diameter
LVDT's	50	0.1-10	0.5 m	0.55 m length cylinder w/ 2 cm diameter

#### 1.1.2 Cylindrical Flexures

A cylindrical flexure (CF) is defined as a flexure with one finite radius of curvature, loaded normal to the plane of curvature. CFs are currently being explored for their potential advantages in geometry, compatibility, and manufacturability to those of existing straight-beam flexure systems. However, up to this point a working model for rules on their elemental analysis and system creation has not been developed. CFs pose a challenge because their mechanics differ

from those of straight-beams. In this paper we are measuring the displacement of a cylindrical flexure given its geometry and material. By measuring the tip and tilt of the flexure in two directions as well as in the direction normal to the plane of curvature, we hope to gain more information about the behavior of cylindrical flexure systems. [2]

Because of their radially symmetric geometry, CF's can be useful for applications such as bearing devices involved in the detection of gaseous plumes. Other applications for CFs are optical systems, laparoscopic tools, and various rotating applications where it is useful to have cylindrical geometry.

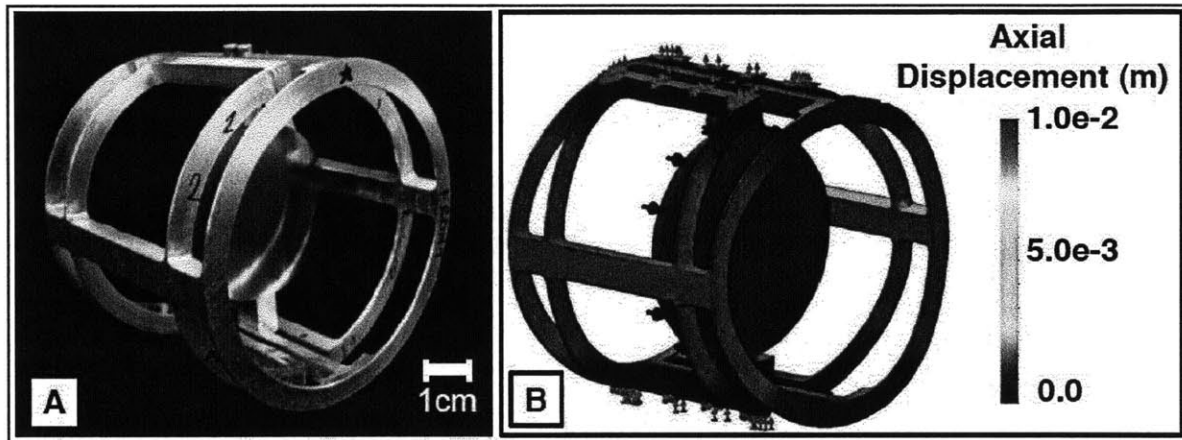


**Figure 1-2:** An example of a cylindrical flexure system (left) and an FEA solid model of a cylindrical flexure system (right). [2].

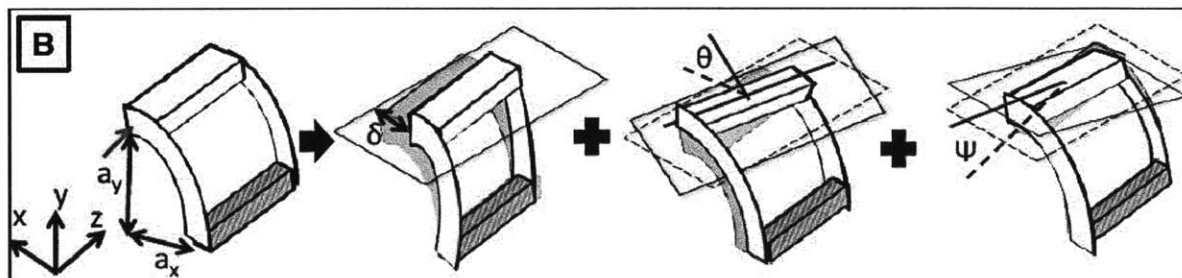


**Figure 1-3:** Diagrams of a loaded cylindrical flexure. It is evident that not only does one see a translation and a rotation as with normal flexures, but a third rotation must be factored in as well. [2]

## **2. Single-Axis Design of Measurement System**

### ***2.1 Signal Layout***

Below is a diagram of the signal transfer through the metrology system. The single-axis implementation of the metrology system consists of a laser diode aimed horizontally at a mirror mounted at an angle on the stage of the CF. The laser is reflected off of the mirror at an angle equal to the incident angle between the laser and the vector normal to the plane of the mirror. This information is useful because movement of the stage on the cylindrical flexure will result either in an increased/decreased laser path or a change in incident angle, depending on the nature of the flexure movement. The reflected laser then is captured by a quadrant photodiode, which outputs up to four currents that are converted to voltage by running them across resistors connected to ground. These outputs are then amplified, and finally compiled and viewed in MATLAB and LabVIEW.

The output of any single quadrant of the photodiode is proportional to the intensity of light on its surface. Therefore, any translation of the laser across the four quadrants of the photodiode (due to movement of the stage) will result in a change in voltage, which we can calculate based on initial conditions and the relationship between the incident angle, mirror angle, and distance between the components.



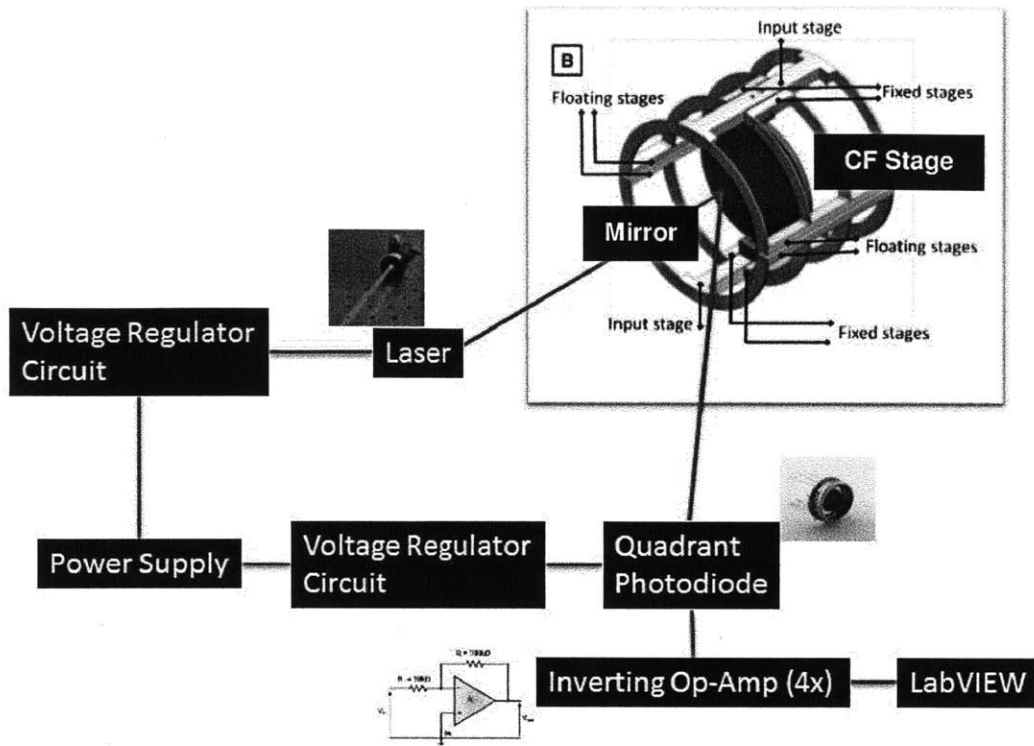


**Figure 2-1:** Diagram of signal transfer from power supply through to LabVIEW installed on Data Acquisition Computer.

## ***2.2 Components***

The data sheets and images of the laser and photodiode are attached in Appendix A. The rest can be found at the websites listed in the references.

### ***2.2.1 Laser***

The laser diode is a model M65051 from US Lasers. It projects a red laser light with a wavelength of 650 nm through an adjustable focus lens. The beam has a power output of 5 mW over either a concentrated point or a more diffuse line. For the purpose of these measurements, the laser was made a line so that more of it could be captured by the sensor's four quadrants. The laser casing is 10.65 mm in diameter.

### ***2.2.2 Quadrant Photodiode***

This model QP5.8-6-TO5 quadrant photodiode from Pacific Silicon Sensor has four quadrant sensors which, as shown in the image below, each output a current proportional to the light intensity on their surface. Operated at a reverse operating voltage of 10 V, for light with a wavelength of 633 nm, these photodiodes have a responsivity of 0.4 A/W. The sum of the widths of two photodiode quadrants is 2.60 mm.

Each quadrant, separated from the next by a 50 $\mu$ m gap, outputs a current, but in order to detect a voltage reading we run the output across a 2 k $\Omega$  resistor that is connected to ground. After these outputs are amplified, they are differenced and normalized in order to find a quantity that equates to a voltage increase for translations in the x and y directions. A diagram of this signal processing is shown below. The quadrants of the photodiode are numbered 1-4 going counterclockwise, facing the photodiode sensor side.

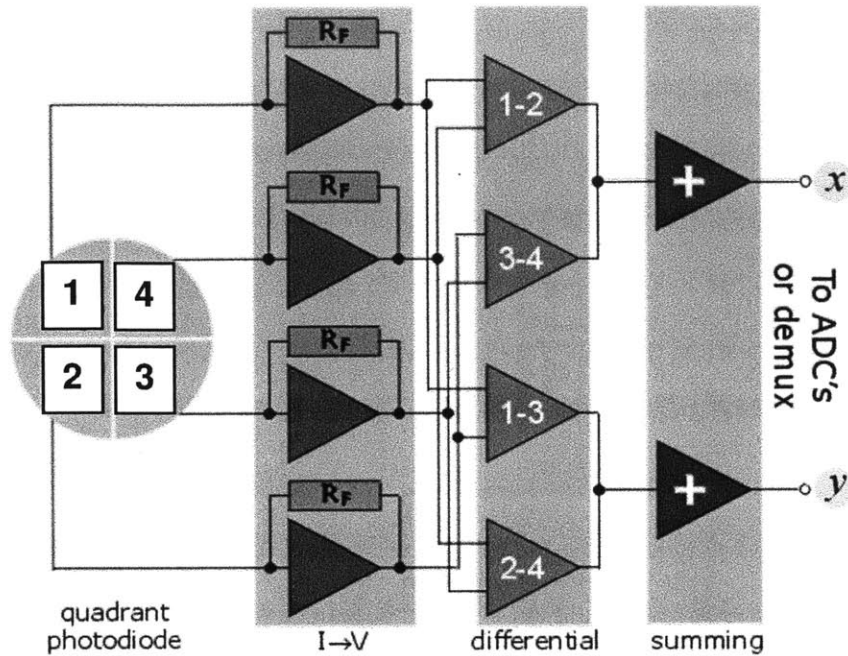


**Figure 2-2:** A diagram in which each output of the quadrant photodiode is converted to a voltage and amplified and differences are summed and averaged in order to find a voltage equivalent to translation in the x and y directions. [3]

If the quadrants are numbered as in Fig. 2-2, the equations for this manipulation of voltage signals are as follows:

$$V_x = \frac{(V_1 - V_4) + (V_2 - V_3)}{(V_1 + V_2 + V_3 + V_4)} \tag{2.2a}$$

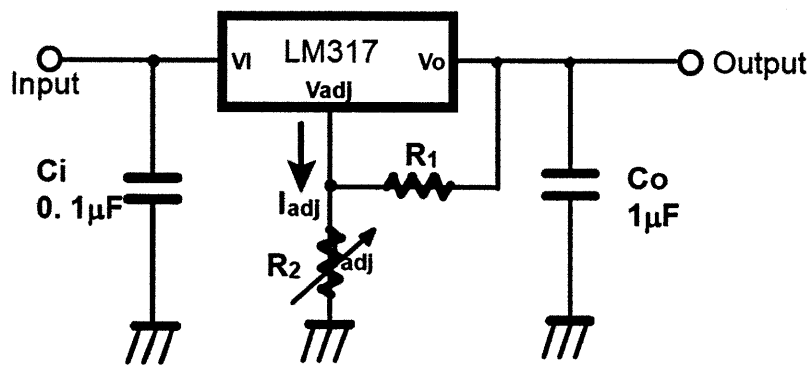
$$V_y = \frac{(V_1 - V_2) + (V_4 - V_3)}{(V_1 + V_2 + V_3 + V_4)} \tag{2.2b}$$

The output level of the laser diode fluctuates and different amounts of light hits the inactive gap between sensors, so the voltages are normalized by dividing them by the total amount of incident light.

### 2.2.3 Voltage Regulator

LM317 3-terminal positive adjustable regulator chips are used to regulate the voltage supply to the laser and the photodiode. Below is a circuit diagram of the voltage regulator, which takes a

DC input voltage and outputs a voltage anywhere from 1.2 to 37 V (based on the resistor values) at a current of 1.5 A. It should be noted that rather than having an adjustable current and voltage with a potentiometer, constant voltages of roughly 3 V for the laser and 10 V for the photodiode are output from the LM317 chip using fixed resistor values of  $R_1^L = 150 \Omega$  and  $R_2^L = 210 \Omega$  for the laser and  $R_1^P = 2 \text{ k}\Omega$  and  $R_2^P = 14 \text{ k}\Omega$  for the photodiode. These values were determined using the equation beneath the diagram below.



$$V_o = 1.25V (1 + R_2 / R_1) + I_{adj} R_2$$

**Figure 2-3:** Diagram of the voltage regulator circuit used to supply constant voltage to the laser and each quadrant of the photodiode [4]

#### 2.2.4 Operational Amplifier

In order to amplify the output voltage of the quadrant photodiode, a non-inverting op-amp circuit with a gain of 3 is used for each quadrant. In the final design, a quadrille op-amp chip is used for each photodiode, and each of the quadrant outputs is amplified. The gain is achieved with fixed resistor values of  $R_3 = 100 \text{ k}\Omega$  and  $R_4 = 200 \text{ k}\Omega$ , for each op-amp circuit. Below are diagrams of the individual non-inverting op-amp circuit and the layout of the op-amps within the LM324 quadrille chip.

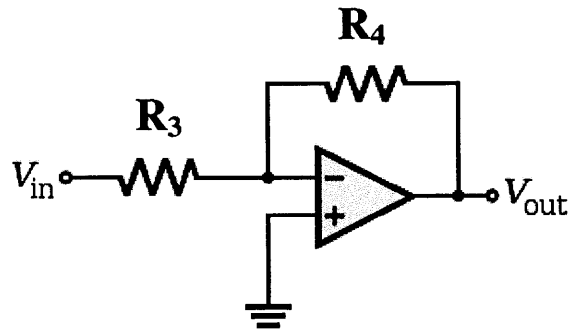


Figure 2-4: Diagram of non-inverting operational amplifier circuit. [5]

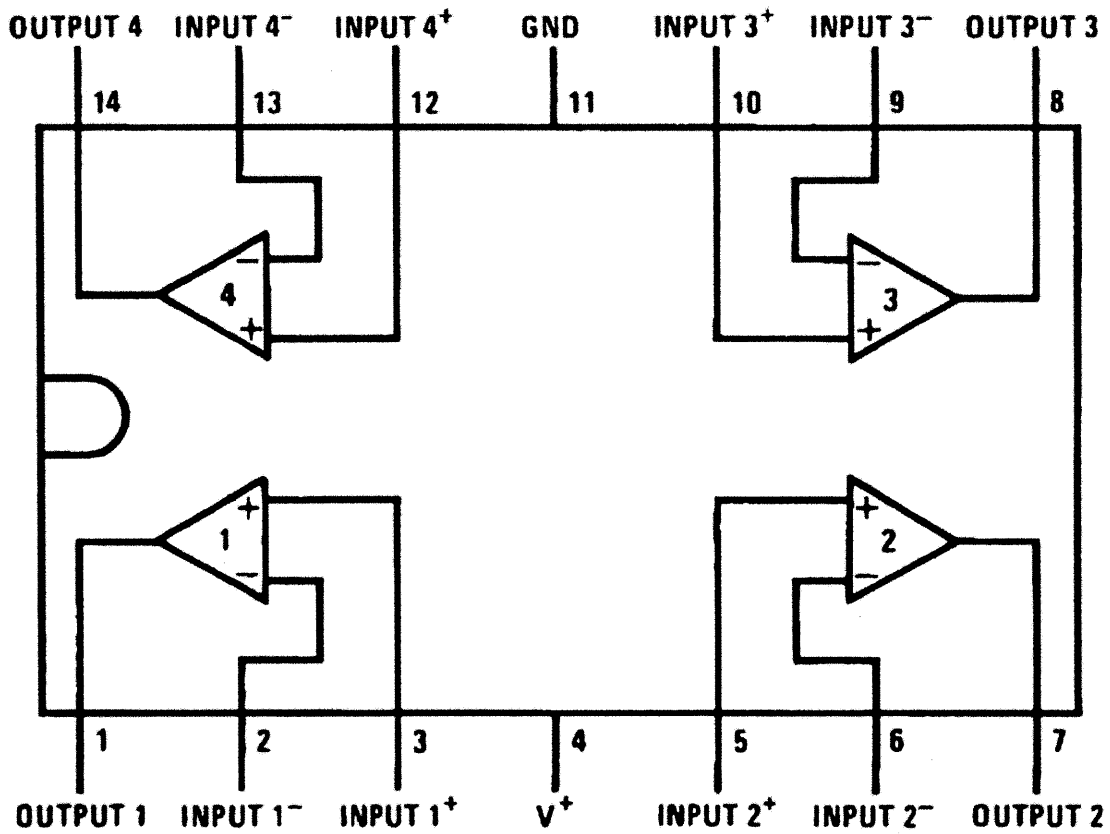


Figure 2-5: Layout of operational amplifiers within LM324 chip. [6]

### **3. Calibration of Measurement System**

#### ***3.1 Calibration Setup***

In order to find the range and resolution of our system in  $\mu\text{m}$  and  $\mu\text{radians}$ , a calibration constant relating voltage to  $\mu\text{m}$  of translation across the surface of the photodiode must be found. In order to find this constant, a separate setup in which the laser was aimed directly at the photodiode (normal to the surface) is constructed. In this setup, the laser and photodiode are placed in simple stands cut out of 6.35 mm (.25 in) acrylic. The photodiode stand is attached directly to the table, while the laser stand is attached to the top of a stage that is actuated by a micrometer. By using the micrometer to translate the laser stand (and thus the laser) in the plane parallel to the photodiode at regular, discrete intervals, as well as recording the differences in output voltages from each quadrant, we can empirically determine the conversion factor.

One challenge of this setup was the imprecision of the stands in being able to aim the laser at a consistent spot on the photodiode. Because of the inability to adjust the direction of the laser and position of the photodiode in multiple axes on a finer scale, the repeatability of the experiment with this element of control proved challenging. This problem is addressed later in the design of more robust flexure stands for the photodiode and laser, which were used for recalibration of the system.

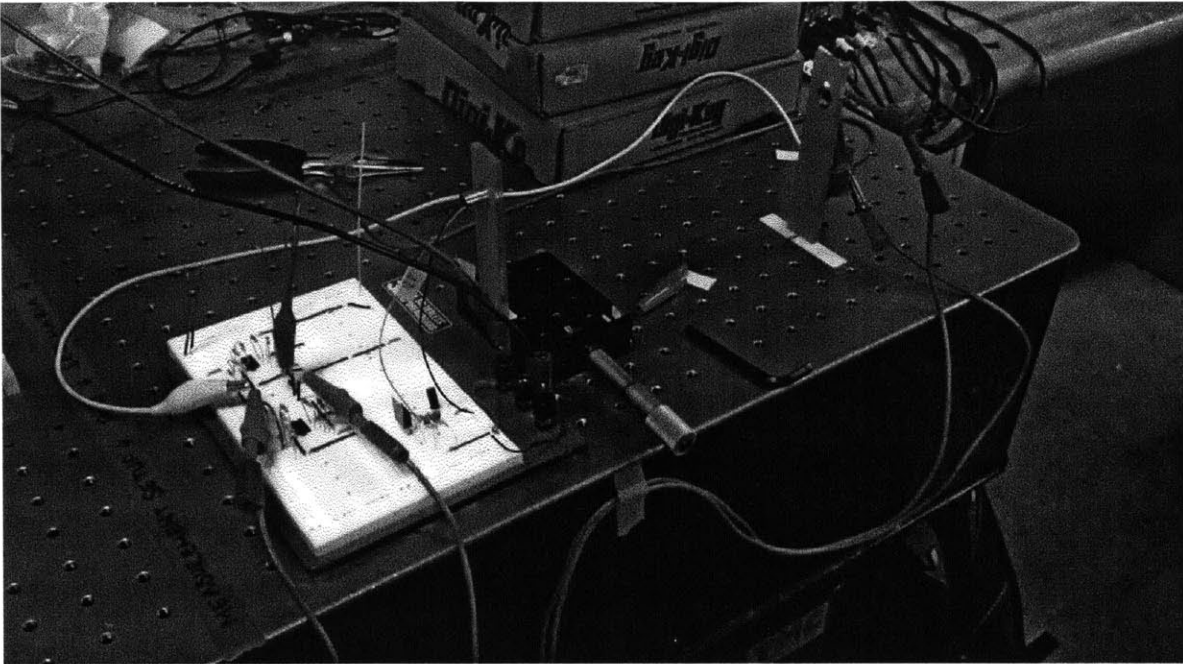


**Figure 3-1:** A picture of the original single-axis setup. The laser sits on a stage which is actuated by a micrometer.

### ***3.2 LabVIEW Program***

The program written in LabVIEW consists of four signals taken from a Data Acquisition manager at a sampling rate of 1 kHz and a buffer size of 10k samples. These four signals are then differenced, summed, and normalized according to the equations 2.2a and 2.2b above, which produces two normalized voltages,  $V_x$  and  $V_y$ . Next, these signals are run through a Butterworth low-pass noise filter with a sampling rate of 1 kHz and a cutoff frequency of 10 Hz. Finally, the signals are output to graphs as well as written to spreadsheet files (along with the raw data as well) with a '.lvm' extension. These files are then imported into MATLAB using a file called 'lvm\_import.m' which can be obtained from The MATLAB Central File Exchange [7]. The block diagram can be found in the Appendix.

### 3.3 System Noise

When the laser was aimed directly at the center of the diode, the noise of the system was recorded to be roughly 90 mV peak-to-peak. In order to determine the limit of our system's resolution, we had to determine whether this noise was actually from the photodiode sensor or being dominated by some other factor such as mechanical noise, ambient light, etc. This 90 mV of noise came from the system which had the analog gain of 3, so an experiment was performed to see if this was analog noise or digital noise. To check, a source of noise was taken from the Data Acquisition (DAQ) device alone, with all of the channels grounded. This device is a NI 9215 Analog Input Module, with 4 input channels. If the noise from the DAQ were much less than 90 mV, we would know that the noise were analog and being amplified by our op-amp circuit. To measure the noise of this device we connected to ground all the channels on the device that we were taking data from, and recorded the resulting summed and normalized signal. The resultant plot is shown below:

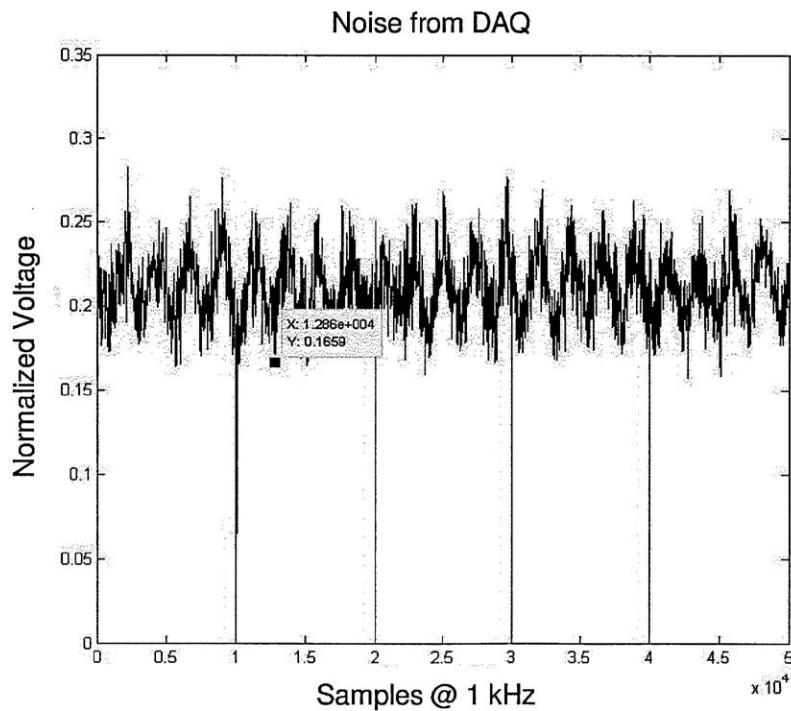


**Figure 3-2:** A plot of the noise from the DAQ board, with a peak-to-peak voltage of near 90 mV.



It is apparent from the plot that the noise from the DAQ was actually roughly 90 mV. This showed us that the noise of the system is dominated by the DAQ, and is the limit of our system's measurement capability. However, this also meant that we could increase the analog gain of our system (within the limits of our power supply) without increasing the noise.

### 3.4 Calibration Results – Photodiode Resolution

Below is a noise-filtered plot of data taken from translating the laser across the width of the photodiode. The laser was actuated by hand in 254  $\mu\text{m}$  (0.010 in) intervals.

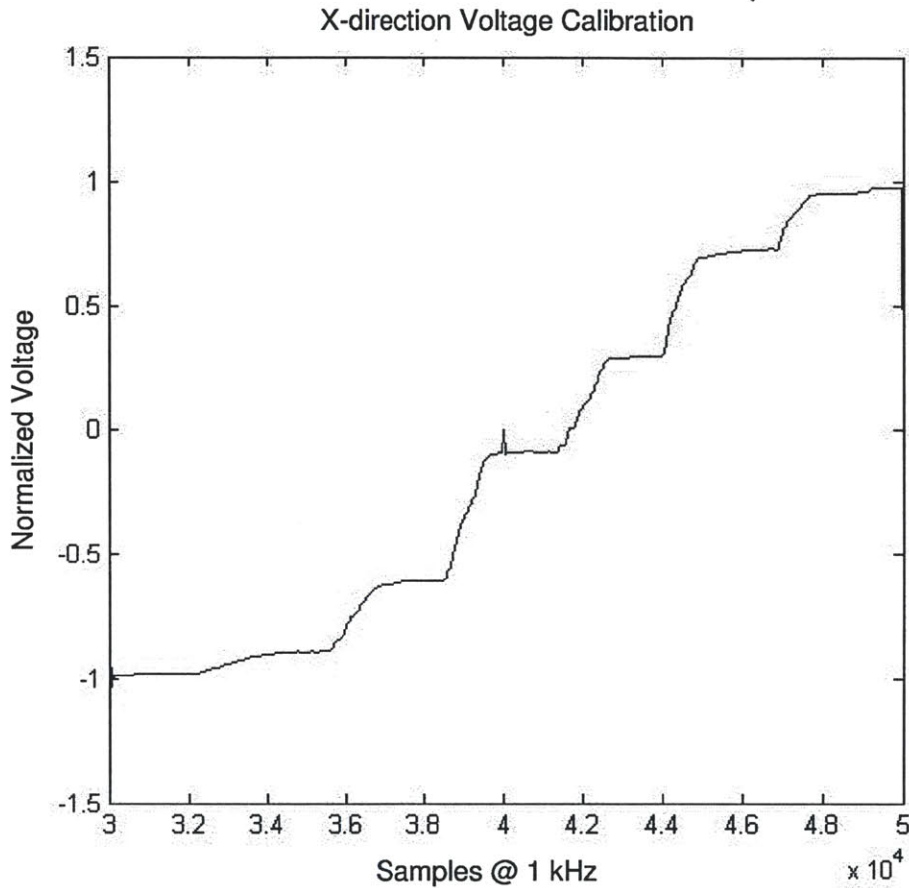


**Figure 3-3:** A calibration plot, where the laser translates in the horizontal direction at 254 micron intervals.

The equation for calculating the calibration constant  $C$  is as follows:

$$C = \frac{k_A \Delta d_{step}}{\Delta V_{step}} \quad (3.4a)$$

where  $k_A$  is the analog gain due to the amplifier,  $\Delta d_{step}$  is the interval distance by which we translated the laser, and  $\Delta V_{step}$  is the change in normalized voltage due to this translation. The change in voltage at a gain of 3 was found to be about 0.51 V, which produces a constant of

$C = 1494 \mu\text{m}/\text{V}$ . From here we can calculate the pre-gain resolution of the photodiode by multiplying this constant by the minimum noise of the system, 90 mV, giving us a resolution of 134 microns. While we can adjust the gain to give us a more readable system resolution, this is the absolute minimum we can see with the photodiode.

## **4. Multiple-axis Design of Measurement System**

### ***4.1 Flexure Stands***

Properly centering the laser on the photodiode at the beginning of measurement requires two different types of flexure systems as stands that would hold and be able to adjust the component within it, be it the laser or the photodiode. Each flexure stand has two different degrees of freedom, combining for a total of four degrees of freedom available for the laser beam to center on the face of the photodiode.

#### ***4.1.1 Laser Stand***

The laser's stand, an isometric model view of which is shown below, is able to rotate the casing to a desired range of 1.5 degrees in two directions. The desired constraints required that rotation of the casing would not exceed a third of the yield stress of the material,  $\sigma_y$ .

##### ***4.1.1.1 Design Iteration 1***

A single part cut out of 6061-T6 aluminum 38.1 mm (1.5 in) box extrusion, slots of 6.35 mm (0.25 in) in width are cut out of each side to create a rectangular notch joint [8] in the center of the part. The photodiode itself is housed in a hole in the center, inserted through the back. These flexures are adjusted using two set screws each on the front and back sides of the piece.

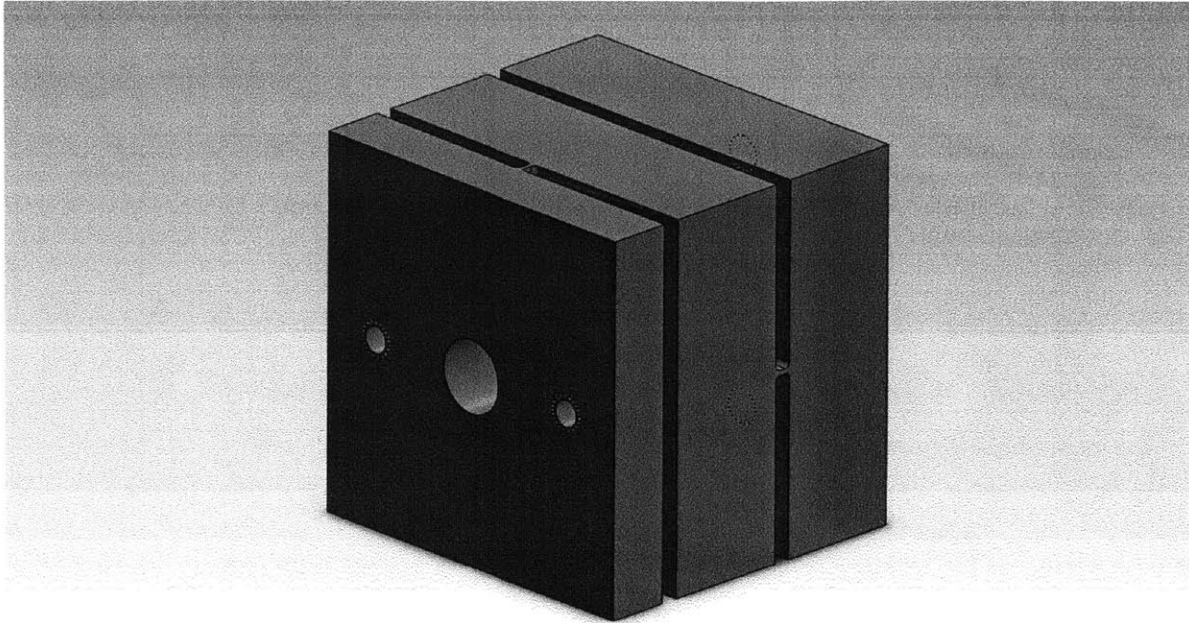


**Figure 4-1:** Solid model original single-part design of the laser stand flexure, to be machined out of square aluminum extrusion.

As shown in the equation and diagram below, the stress in the beam in bending is a function of the thickness of the beam. The maximum stress in the hinge is given by

$$\sigma_{max} = \frac{Et}{4a_x} \theta_{desired} \tag{4.1a}$$

Where  $E$  is the Young's modulus of the material and  $\theta_{desired}$  is the maximum angle to which the flexures would bend. The dimensions and material properties of the hinge are shown as marked in the image and table below.

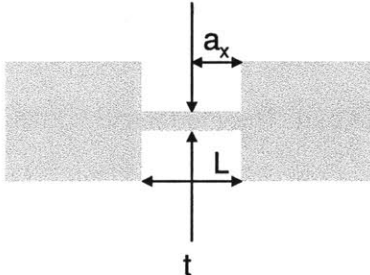


**Figure 4-2:** A profile view of a rectangular notch hinge. [8]

**TABLE 4-1:** The properties of 6061 T6 Aluminum and the first design iteration of the rectangular notch hinge. [9]

	Symbol	Value
Young's Modulus of 6061 T6 Aluminum	$E$	68.9 GPa
Yield Stress of 6061 T6 Aluminum	$\sigma_y$	276 MPa
Desired maximum deflection of beam	$\theta_{desired}$	1.5 deg
Characteristic length of beam	$a_x$	3.175mm (0.125 in)
Thickness of beam	$T$	0.508mm (0.020 in)
Maximum Stress in beam	$\sigma_{max}$	96.203 MPa

We chose not to use this design mainly because fabrication of the part with a thickness of 0.508 mm (0.020 in) that would fit the desired constraints was impractical and often inaccurate. However, this design does fit the requirements well and would be a desirable goal in further refinement of the system.

#### 4.1.1.2 Design Iteration 2

In order to find a more DFM-centric design, our next design would be an assembly rather than a one-part piece. The material chosen for the new flexure was A1095 blue spring steel. As shown in the model, two pieces of 0.178 mm x 6.35 mm x 25.4 mm (0.007 in x 0.25 in x 1.0 in) spring steel are inserted and bonded into pieces of acrylic of 6.35 mm thickness. The acrylic is then bonded to an attachment piece that can be mounted to an L-bracket or the optical table. This design ensures that the thickness of the beam is accurate and small enough to maintain flexibility without too much stress in the part. The model and equations for the deflection of these flexures are shown below.

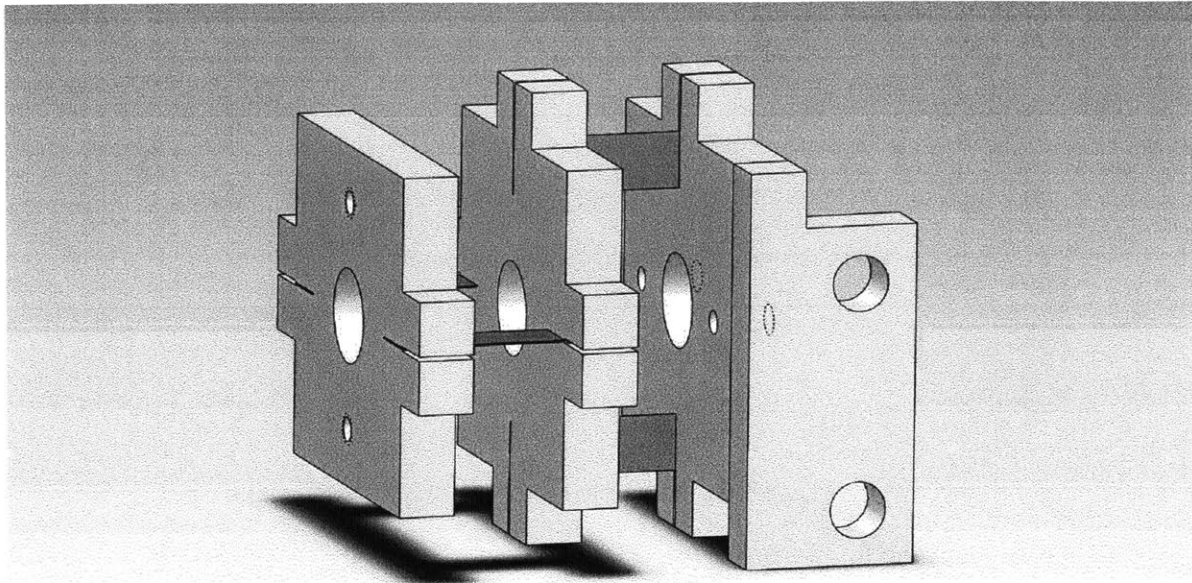


**Figure 4-3:** Redesign of the laser stand flexure, with spring steel in bending, bonded to acrylic pieces.

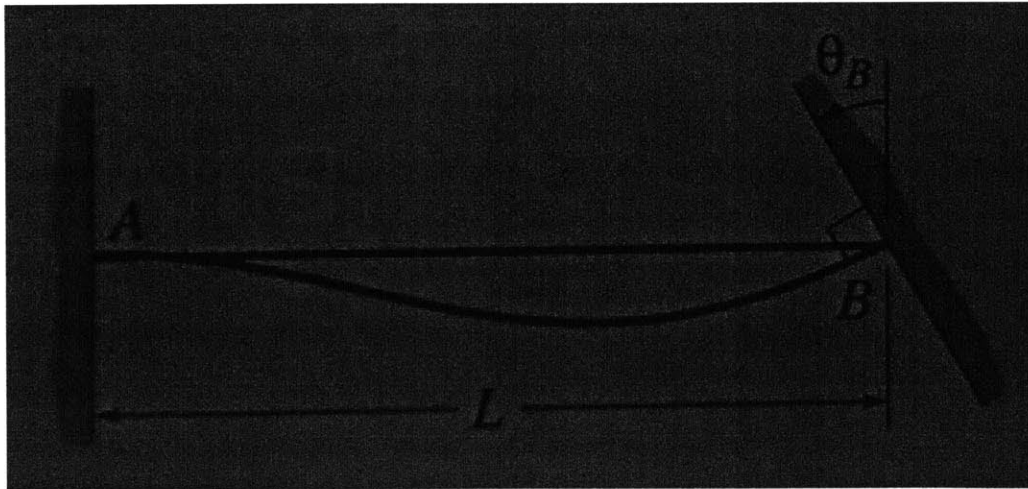


**Figure 4-4:** A profile view of the flexure found in the second design iteration, the highest moment of which can be found at point B when in bending. [10]

The image above [10] shows a shape of the beam in bending with an angle of  $\theta_B$ , which is the same angle as our  $\theta_{desired}$ . The moment at point B can be expressed as

$$M_B^l = \frac{4E_{ss}I}{L} \theta_{desired} \quad (4.1b)$$

where  $L$  is the length of the beam between the two pieces and  $I$  is the polar moment of inertia of the beam [10]. Combined with the equation for stress of the beam

$$\sigma_B = \frac{M_B^l t}{I} \quad (4.1c)$$

it is apparent that this design falls within the safety factor of a third of the yield stress, as shown in the table characterizing this flexure below.

**TABLE 4-2:** The properties of A1095 Spring Steel and the second design iteration of the rectangular notch hinge. [11]

	Symbol	Value
Young's Modulus of A1095 Spring Steel	$E_{ss}$	200GPa
Yield Stress of A1095 Spring Steel	$\sigma_y$	455MPa
Desired maximum deflection of beam	$\theta_{desired}$	1.5 deg
Characteristic length of beam	$L$	6.35mm (0.25 in)
Thickness of beam	$T$	0.1778mm (0.007 in)
Maximum Stress in beam	$\sigma_B$	146.608MPa

#### 4.1.2 Photodiode Flexure Stand

The photodiode's stand is able to translate it in two directions. This assembly consists of three pieces: a ground, the flexure, and a moving stage. The ground or base piece, mounted to the table, is a square 50.8 mm (2 in) piece of aluminum, with 6.35 mm (0.25 in) of thickness. Mounted to this ground piece are two aluminum flexures, with 50.8 mm long flexing sections of 0.762 mm (0.030 in) in thickness in two directions. Finally, a stage housing the photodiode is mounted to these flexures and is actuated in both directions by four set screws. The bearings have a total of 3 mm of freedom in two directions. Again, the flexure is actuated by rotating two



set screws relative to each other in order to achieve a desired position. To protect against bending outside of the desired range, a stop is fixed on each inner side of the ground piece.

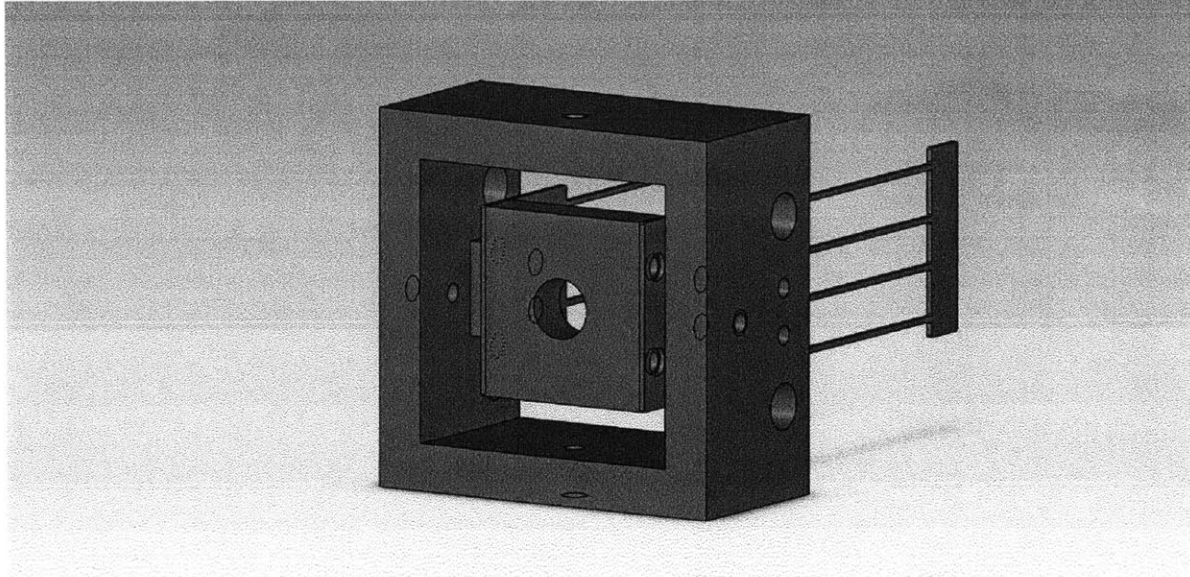


**Figure 4-5:** A solid model of the flexure stand assembly for the quadrant photodiode. There are holes in each side of the base piece for set screws to actuate the stage, as well as larger holes for mounting the stand to an L-bracket or an optical table.



**Figure 4-6:** A profile view of the flexure found in the photodiode stand flexures, the highest moment of which can be found at point B, where there is a deflection of  $\delta_B$ . [10]

$$M_B^P = \frac{6EI}{L^2} \delta_B \quad (4.1d)$$

As shown in equation 4.1d, the moment in the beam is a function of the displacement of the stage which is free and guided at point B. This equation again combined with 4.1c gives us the maximum stress in the beam, 91.613 MPa, given a deflection of  $\delta_B = 1.5$  mm, showing that the range of this flexure is within a safety factor of a third of the yield stress for aluminum.

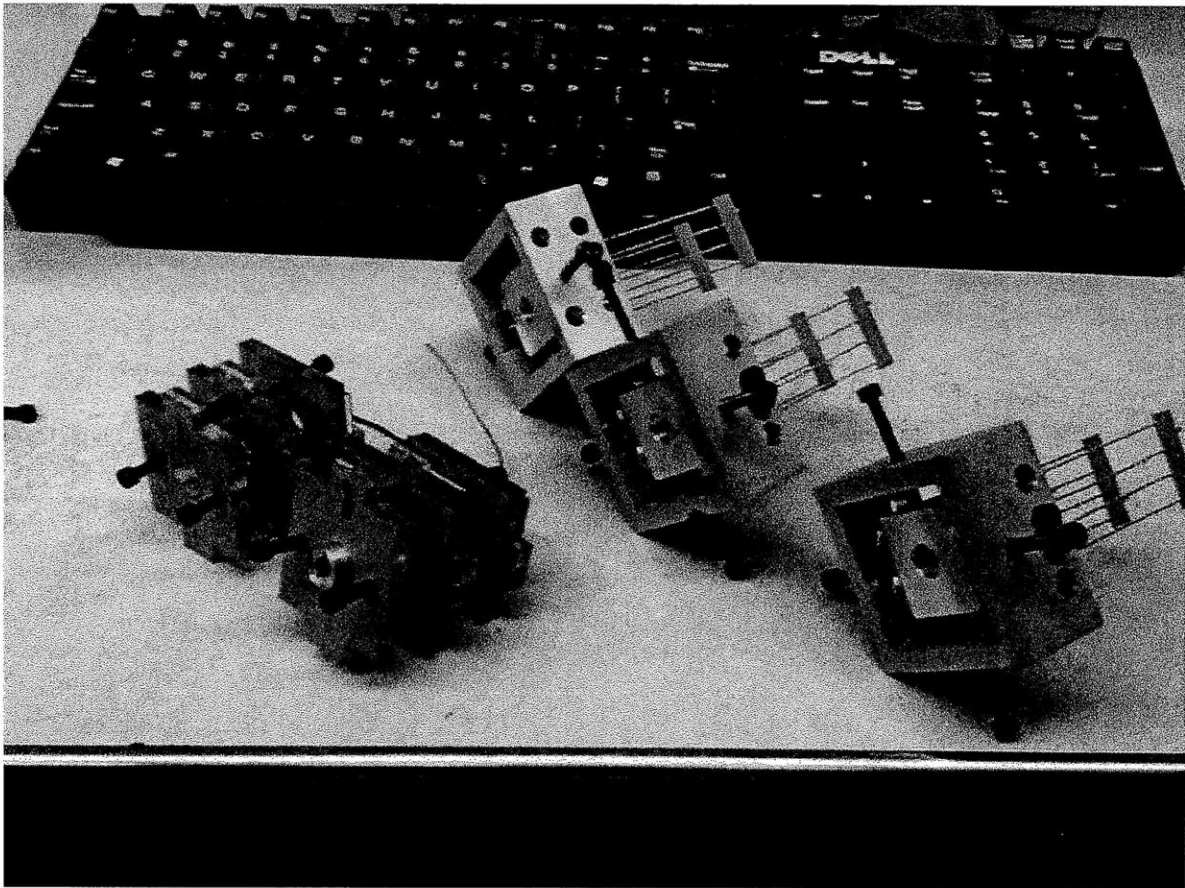


**Figure 4-7:** An image of the assembled flexure stands.

## ***4.2 Angle Functions - Parameter Relations***

In order to detect rotations and translations of the stage in multiple axes, the single-axis design must be multiplied. The desired range of the system was to be able to detect tip and tilt of the stage as well as translations normal to the plane of curvature of the CF. This design has three degrees of freedom, so three laser-photodiode setups are required to fully capture all motions of the system.

### ***4.2.1 Translations of Stage***

The translation of the beam across the surface occurs when either a rotation or translation of the stage happens. Below is an image modeling of the effect of a translation of a single mirror on the reflected laser beam. A study of a singular mirror is useful because a translation of the stage in this manner will produce a reflection—and therefore a distance of translation across the photodiode surface—that is the same for each mirror, given that the mirrors are mounted with the same magnitude of angle.

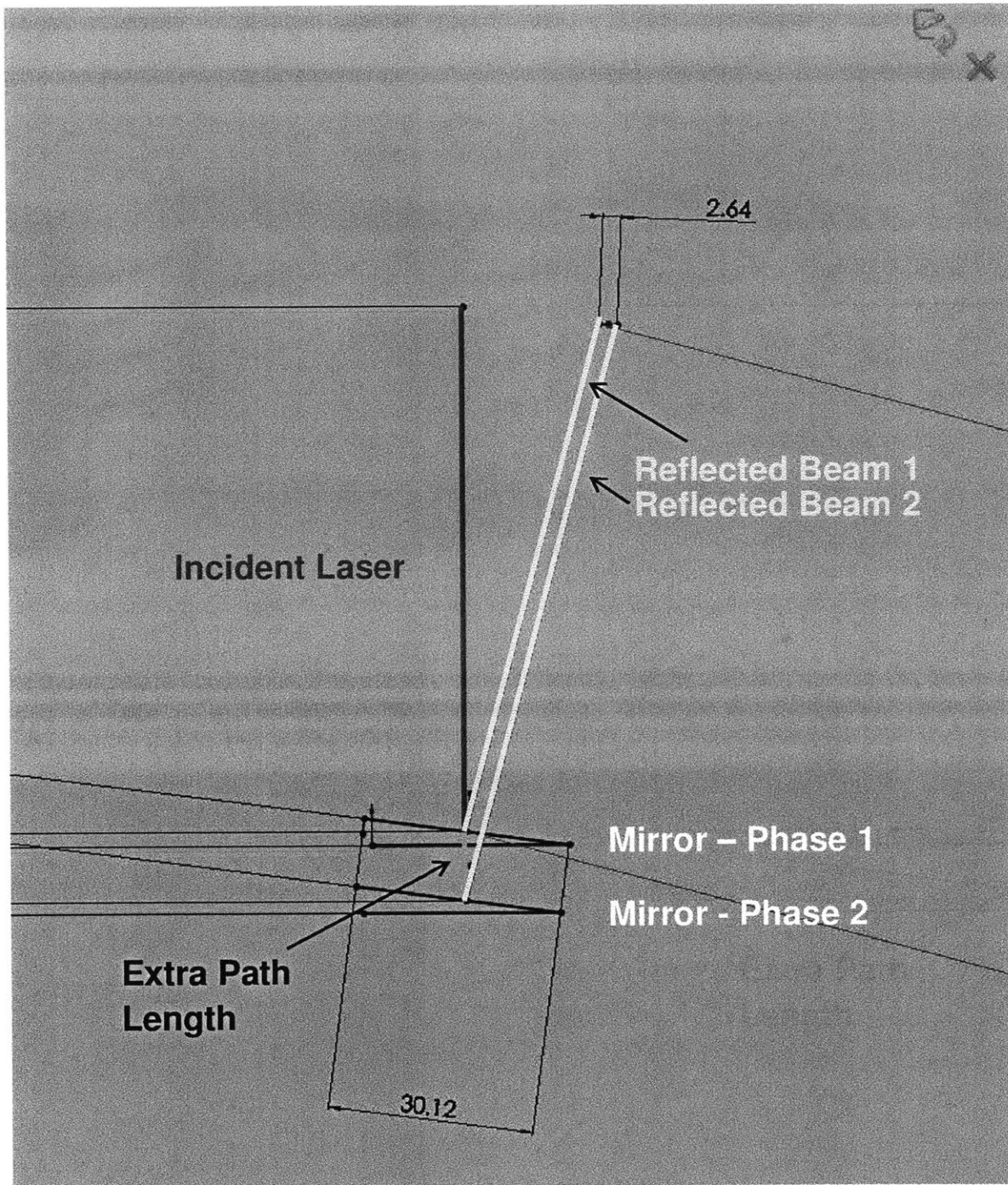


**Figure 4-8:** A modeling of the effect of the translation of the mirror on the reflected laser beam. The red line represents the incident laser. The two sets of pairs of angled, black lines represent the before and after positions of the mirror. The two yellow lines represent the before and after positions of the reflected beam, which are always parallel when the stage translates. The orange line represents the extra path length that the laser travels.

As shown in King's thesis, the amplification of displacement caused by translation of the mirror surface off of which the beam is reflected is a function of the angle of incidence between the laser beam and the mirror surface. Because the laser has a fixed position, the angle of incidence itself is a function of the angle with which the mirror is mounted on the stage of the cylindrical flexure. The equation for the translation of a beam across the surface of a photodiode,  $\delta$ , is given by

$$\delta = \frac{d}{\cos(\theta)} \cos(2\theta - 90) \quad (4.2a)$$

Where  $d$  is the displacement of the reflecting surface and  $\theta$  is the incident angle of the beam and the reflecting surface. As we can see above,  $d$  is equal to the extra path length that the laser has to travel. In this setup, the lasers were positioned such that their beams are perpendicular to the stage, so the incident angle  $\theta$  was in fact equal to the angle at which the mirrors are mounted on the stage.

Because this angle determines the amplification of displacement of the stage—i.e. the ratio of  $\delta$  to  $d$ , it effectively determines the resolution with which we can measure translations of the stage normal to the plane of the cylindrical flexure.

#### *4.2.2 Rotations of Stage*

Translations of the reflected beam due to rotations of the stage depend not only on the angle at which the mirrors are mounted, but also the distance from the target to the photodiode. In order to find this relationship, we sought out again to relate  $\delta$  to the amount of rotation,  $\varphi$ . However, in order to maintain a dimensionless factor of amplification or reduction just as with the translational motion, we related  $\delta$  to  $y$ , the extra path length of the laser due to a rotation of the stage. This extra path length is given by

$$y = r \tan(\varphi) \quad (4.2b)$$

where  $r$  is the radius from the point where the laser is projected onto the stage to the center of rotation of the stage. In order to find  $\delta$  as a function of distance from the target to the photodiode, we related  $\varphi$  to the angle between the incident and reflected beams, both before and after rotation. These angles are  $\alpha_1$  and  $\alpha_2$ , respectively, and the functions for this relation are as follows:

$$\alpha_n = 2\theta_n \quad (4.2c)$$

$$\varphi = \alpha_2 - \alpha_1 \quad (4.2d)$$

Finally, we used these angles to develop a trigonometric relationship between the vertical distance  $D$ —taken from a top view—from the photodiode to the target and the translation of the laser,  $\delta$ . This relationship is given by

$$\delta = D (\tan(\alpha_2) - \tan(\alpha_1)) \quad (4.2e)$$

Now that we have  $\delta$  as a function of the incident angles and the distance from the photodiode to the target, we can relate  $\delta$  to  $y$  in order to find the coefficient of amplification due to rotations of the stage:

$$\frac{\delta}{y} = \frac{D (\tan(\alpha_2) - \tan(\alpha_1))}{r \tan(\varphi)} = \frac{D}{r} (\tan(\alpha_1) \tan(\alpha_2) + 1) \quad (4.2f)$$

Below is a modeling of the effect of a rotation of the stage on a single beam. We see that unlike with translations, the reflected beams are not parallel when the stage is rotated.

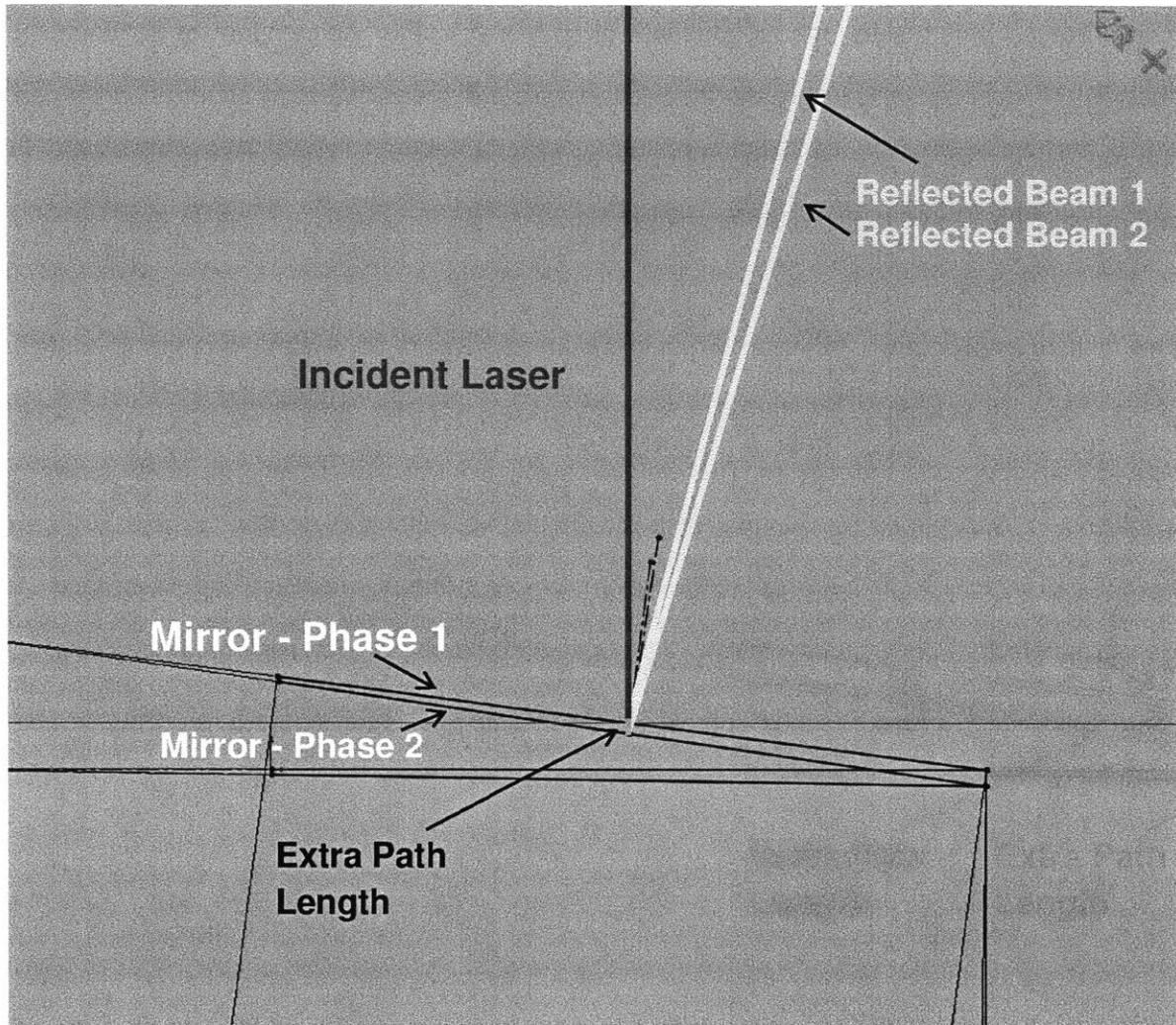


**Figure 4-9:** A close-up angle study of the effect of rotations of the stage on the reflected beam, with the same labeling as Fig. 4-8. Because of the amplification of the angle with distance, the range of rotation—and therefore the extra path length of the laser—is much smaller.

#### 4.2.3 Multiple-Axis Rotations

In order to differentiate tip and tilt from translations, we needed to have at least two mirrors at angles in two different directions. This is because a rotation of the stage will result in two differing  $\delta$ 's, one for each reflected beam, whereas a translation of the stage would produce the same magnitude of  $\delta$  albeit in two different directions. The simplest case is when two mirrors are mounted such that one is mounted at an angle to the vertical and the other at an angle to

the horizontal. This makes one independent of tip and the other independent of tilt, because each has at least one axis where the incident angle is 0 degrees. With this information we can find rotations in the tip and tilt simply by using equation 4.2e above, you can use the known  $D$  and  $\alpha_1$  and measured  $\delta$  to find  $\alpha_2$  for each direction.

This method breaks down, however, when you want to measure combinations of the tip and tilt of the stage. The simplest counterexample is that in which a rotation of the stage across a 45 degree angle opposite the mirrors. This would result in both beams moving inward or outward the same distance, and would thus be indistinguishable from a translation. It is for this reason a third mirror is needed at a different angle to indicate these combinations of rotation. The method for finding the amount of rotation around a given axes does not change, we simply have a new axes that we can measure, thus completing the set of axes we wanted to be able to see rotations in.

#### *4.2.4 Mirror Mounting*

Mirrors of silicon pieces are mounted to the flexure stage using right-triangular pieces of acrylic with angles of 14.725 degrees each. Three of these pieces are glued to the stage, one at a horizontal angle facing left, one at a vertical angle facing downward, and one at a 45 degree angle facing down and to the right. The mirrors were then mounted to the acrylic with glue. These placements were chosen for reasons above. The angle of each triangle was optimized for resolution, as shown in the section below.



### 4.3 Range and Resolution

In order to find the translational range of motion of the stage, we must reduce the amplification of the translation down to

$$\frac{\text{resolution of photodiode}}{\text{width of photodiode}} = \frac{\delta}{d} = \frac{\text{width of photodiode}}{\text{system translational range}} \quad (4.3a)$$

This is because the reduction results in a change in the how much the laser moves given a certain movement of the stage. For example, a movement of 1 micrometer of the stage would result in even smaller movement on the surface of the photodiode. Therefore, the translational range of the overall system does depend on the resolution with which the photodiode can measure a translation across its surface. In order to optimize the resolution of the system, we must find the smallest length that the photodiode can measure.

As calculated earlier, the smallest resolution that the photodiode can handle is 134  $\mu\text{m}$ . Using equation 4.3a above, we found that the total translational range of the system is 5.04 cm, and using equation 4.2a above we found that the optimal angle at which to mount the mirrors for this reduction is 14.725 degrees.

The rotational range of motion of the stage can be found in a similar manner to that of the translational range: by scaling the ratio of the translation of the laser to the extra path length it travels.

$$\frac{\text{resolution of photodiode}}{\text{width of photodiode}} = \frac{\delta}{y} = \frac{\text{width of photodiode}}{\text{system rotational range}} \quad (4.3b)$$

So we see that the theoretical system rotational range is also 5.04 cm, which translates to +/- 33.5 degrees, given a radius  $r$  of 38.1 mm (1.5 in). However, in this case our desired range is only around 1 degree of rotation. Using this information and the angle found for optimizing

translational resolution, we chose to place the photodiode 50.8 mm (2 in) away from the surface as to fit the 25.4 mm (1in) spacing of the optical table and to capture this range of 1 degree, though the optimal distance for capturing the range would be 58.5 mm (2.30 in).

# 5. Conclusion

## 5.1 Overview

This paper has shown the plausibility and development of a three-axis laser metrology system, which has inherent advantages in cost and simplicity over other metrology systems whilst maintaining precision and range. The signal flow from the power supply through the laser and photodiode into LabVIEW was laid out in detail, along with each component of the circuit and the analog and digital manipulations of the signal. A calibration constant of 498 microns per volt was found for our system, and the pre-gain resolution of the photodiode output was found to be 134 microns due to a limiting factor of 90 mV of noise from the DAQ. In order to achieve a precise measurement of this constant, a way of acutely adjusting the direction and position of the laser and photodiode was developed through the use of different flexures. Finally, a set of geometric characteristics was given for the path of the laser given a translation or rotation of the stage.

Below is a table summarizing the cost and performance of the system. Given that the system measures movement in three axes and flexibly measures parts both statically and dynamically, it is an economical choice in the measurement of small parts.

**TABLE 5-1:** A cost-performance analysis of the designed metrology system.

	Resolution (pre-gain)	Estimated Price	Range	Size
Laser System	134 $\mu$ m	\$400.00	5.04 cm	0.5m x 0.5 m

## **5.2 Future Work**

This system is currently used for measuring cylindrical flexures, but could quite feasibly measure other flexure systems with greater ranges of motion. 5 cm is quite large given such a small resolution.

Because this amount of noise seems high, it would be beneficial to characterize the sources of noise. Performing a Fourier transform over a noise signal and finding the resonant peaks would help us know what types of noise are affecting the system. Ideally, we'd like to limit the noise of the system to solely that of the photodiode, so that rather than having the resolution of the photodiode as limited by some other element of our system, we would have the resolution as limited by its own output.

It would also be beneficial to explore various other materials for use in the flexure stands, especially for the photodiode stand. Given the materials available and the constraints of having the same stiffness in both directions, it was non-trivial finding a robust and flexible design for the flexure. Using a different material would almost certainly increase the range of motion.

## **6. Appendices**

### **Appendix A: Data Sheets**

Located in this Appendix are the data sheets for the laser diode (U.S. Lasers) and photodiode (Mouser Electronics). The laser datasheet contains information about the optical characteristics of the laser, including the size of the aperture, wavelength. Also included are the operating conditions of the laser. The photodiode datasheet also contains this component's typical operating conditions and maximum ratings. Also useful in this data sheet is a curve describing the responsivity of the photodiode given a certain wavelength of light, should one desire to change the laser used in this system for greater responsivity. Both datasheets contain the dimensions of each component.

# Laser Data Sheet [12]

Page 1 of 1

Laser Diode - D660nm5mw

Back to **M650-5** **EPM650-5**

**DATA SHEETS .... EPM & M650nm 5mW ....RED LASER MODULE**

<b>Barrel Specs:</b> <ul style="list-style-type: none"> <li>• 3/8 - 56 Thread Size</li> <li>• Dia: 10.4mm</li> <li>• Length: 17mm</li> </ul>	<b>Collect Specs:</b> <ul style="list-style-type: none"> <li>• 3/8 - 56 Thread Size</li> <li>• 4.3mm Aperture</li> <li>• Half Hard Brassbbb</li> </ul>	<b>Lens Housing Specs:</b> <ul style="list-style-type: none"> <li>• 3/8 - 56 Thread Size</li> <li>• 3.7mm Aperture</li> <li>• 7mm Plastic Lens</li> </ul>
--	--	---

**RED LASER DIODE ABSOLUTE MAXIMUM RATINGS - (Tc=25 °C)**

<b>TECHNICAL DATA</b> Visible light output                    650nm Optical power output                    5mW CW Package Type                                5.6mm Built-in photo diode for monitoring laser output	<p><b>Pin Out Diagram - Style A</b></p>
---	---

Items	Symbols	Values	Unit
Optical output power	Po	5	mW
Laser diode reverse voltage	V	2	V
Photo diode reverse voltage	V	30	V
Operating temperature	Topr	-10 ~ +60	°C
Storage temperature	Tstg	-40 ~ +85	°C

**OPTICAL and ELECTRICAL CHARACTERISTICS - (Tc=25 °C)**

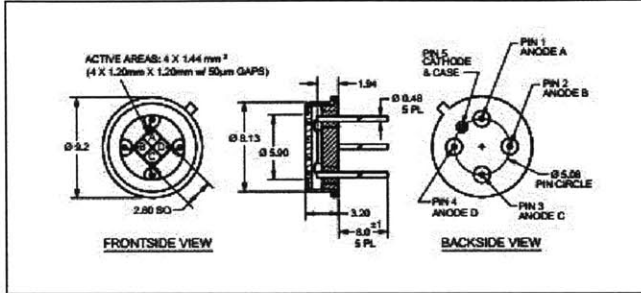
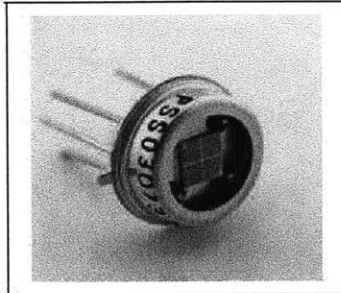
Items	Symbols	Min.	Typ.	Max.	Unit	Test Condition
Optical output power	Po	-	5	-	mW	-
Threshold current	Ith	-	20	40	mA	-
Operating current	Iop	-	40	60	mA	Po=5mW
Operating voltage	Vop	-	2.7	-	V	Po=5mW
Lasing wavelength		645	650	655	nm	Po=5mW
Beam divergence		-	5	11	deg	Po=5mW
Beam divergence		-	25	37	deg	Po=5mW
Monitor current	Is	-	10	20	uA	Po=5mW
Astigmatism	As	-	11	-	um	Po=5mW
MTTF			10000 hrs			Po=5mW
Emitter Size		10 x 60 Microns - Emitter Distance to Cap Lens = 0.3mm				
Structure		Index Guided				

<http://www.nvginc.com/d650nm5m.htm> 4/3/03

# Quadrant Photodiode Data Sheet [13]



## Pacific Silicon Sensor Quadrant Series Data Sheet Part Description QP5.8-6-TO5 Order # 03-073



### FEATURES

- 4 X 1.20 mm square active area
- Small gap
- Low dark current
- High resolution

### DESCRIPTION

4 X 1.44 mm<sup>2</sup> Low Dark Current Quadrant Photodiode with P on N construction and 50 µm gaps. Hermetically packaged in a TO-5 with a clear borosilicate glass window cap.

### APPLICATIONS

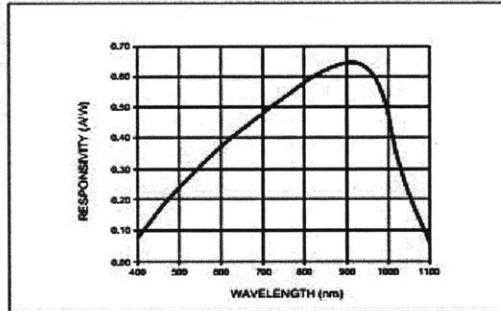
- Laser beam position sensor
- Autocollimators
- Optical tweezers
- Ellipsometers



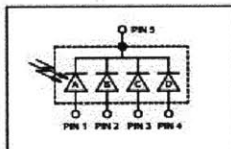
### ABSOLUTE MAXIMUM RATING

SYMBOL	PARAMETER	MIN	MAX	UNITS
T <sub>STG</sub>	Storage Temp	-55	+125	°C
T <sub>OP</sub>	Operating Temp	-40	+100	°C
V <sub>REV(O)</sub>	Reverse Operating Voltage	-	50	V
I <sub>PEAK</sub>	Peak DC Current	-	10	mA

### SPECTRAL RESPONSE



### SCHEMATIC



### ELECTRO-OPTICAL CHARACTERISTICS @ 22° C

SYMBOL	CHARACTERISTIC	TEST CONDITIONS	MIN	TYP	MAX	UNITS
I <sub>0</sub>	Dark Current*	V <sub>R</sub> = 10 V	—	0.4	—	nA
C	Capacitance*	V <sub>R</sub> = 10 V	—	—	5.5	pF
	Responsivity	V <sub>R</sub> = 0 V; λ = 633 nm	—	0.40	—	A/W
		V <sub>R</sub> = 0 V; λ = 900 nm	—	0.64	—	
V <sub>BR</sub>	Breakdown Voltage	I <sub>0</sub> = 10 µA	—	15	—	V
t <sub>r</sub>	Rise Time	V <sub>R</sub> = 10 V; λ = 850 nm; R <sub>L</sub> = 50 Ω	—	20	—	ns
	Uniformity of Sensitivity	V <sub>R</sub> = 10 V; λ = 880 nm	—	±1	±2	%

\* per element

Disclaimer: Due to our policy of continued development, specifications are subject to change without notice.

### USA:

Pacific Silicon Sensor, Inc.  
5700 Corsa Avenue, #105  
Westlake Village, CA 91362 USA  
Phone (818) 706-3400  
Fax (818) 889-7053  
Email: [sales@pacific-sensor.com](mailto:sales@pacific-sensor.com)  
[www.pacific-sensor.com](http://www.pacific-sensor.com)

### International sales:

Silicon Sensor International AG  
Peter-Behrens-Str. 15  
D-12459 Berlin, Germany  
Phone +49 (0)30-63 99 23 10  
Fax +49 (0)30-63 99 23 33  
Email: [sales@silicon-sensor.de](mailto:sales@silicon-sensor.de)  
[www.silicon-sensor.de](http://www.silicon-sensor.de)

Proud Members of the Silicon Sensor International AG Group of companies

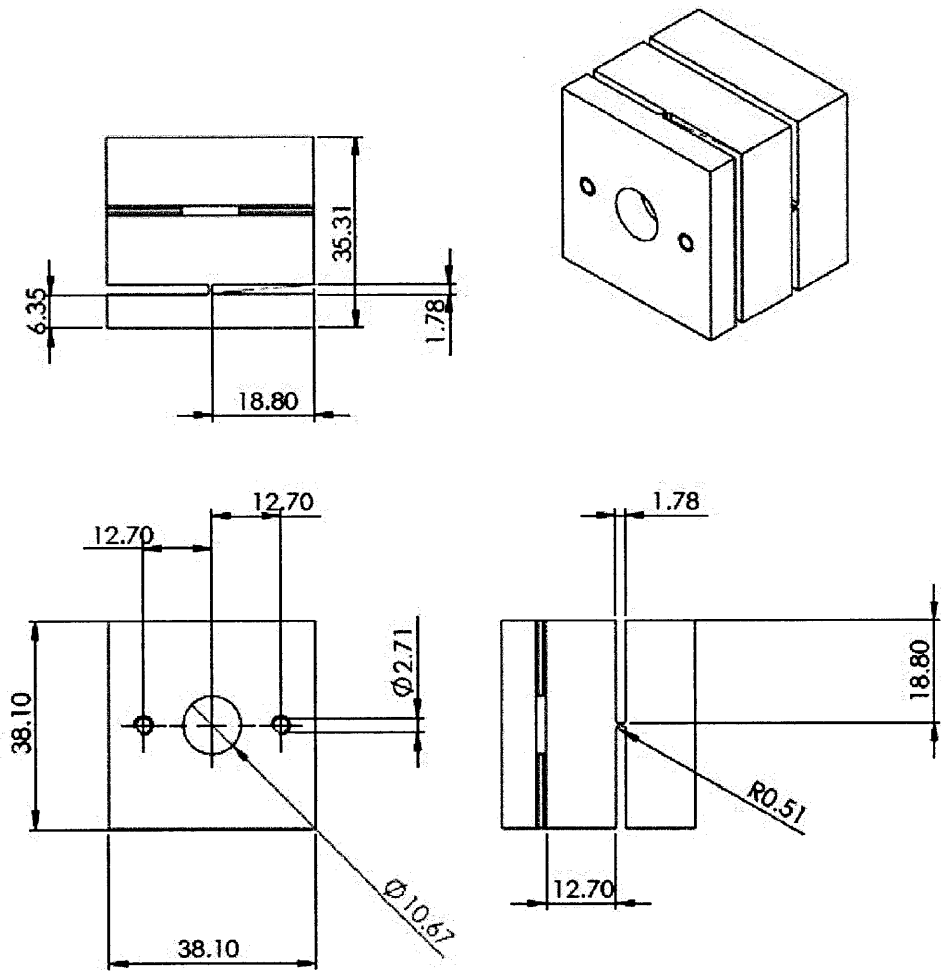
10/29/2010

## **Appendix B: Technical Drawings**

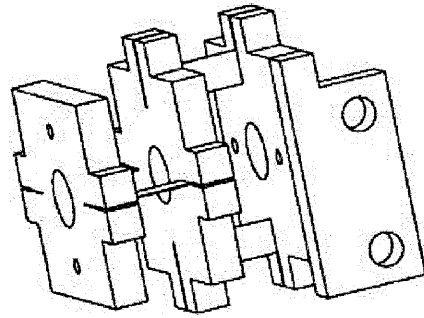
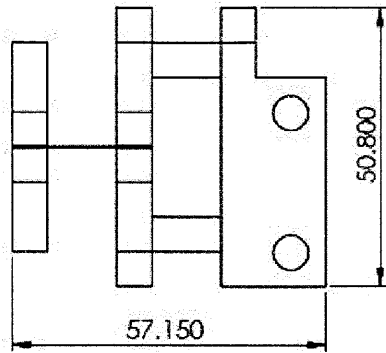
Below are the technical drawings for each of the flexure stands in our system, including the original and redesign of the laser stand flexure. The drawings contain the dimensions (in mm) and material used in the current system for each part in each assembly, as well as a perspective drawing of each assembly, so that these stands can be reproduced or redesigned.



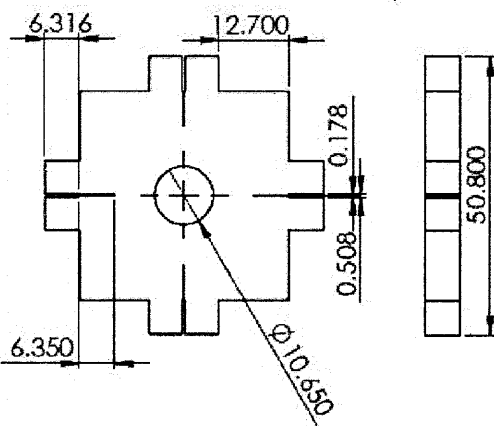
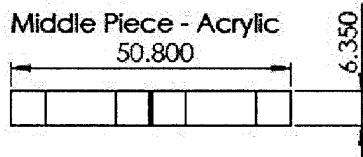
Laser Stand v1 - 6061 T6 Aluminum



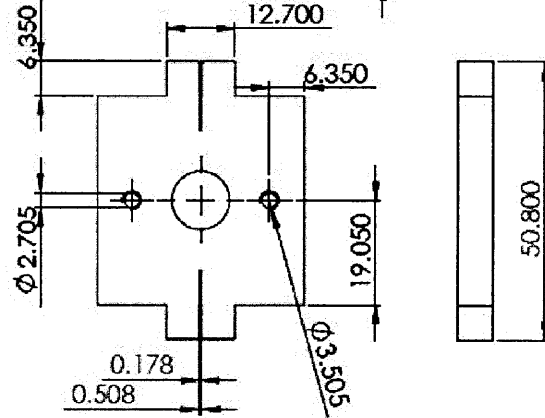
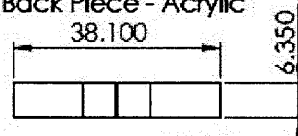
Laser Stand v2



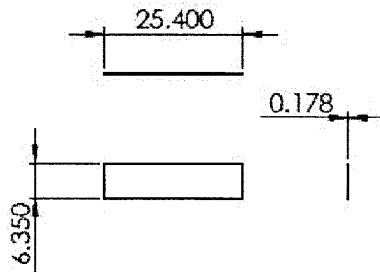
Middle Piece - Acrylic  
50.800



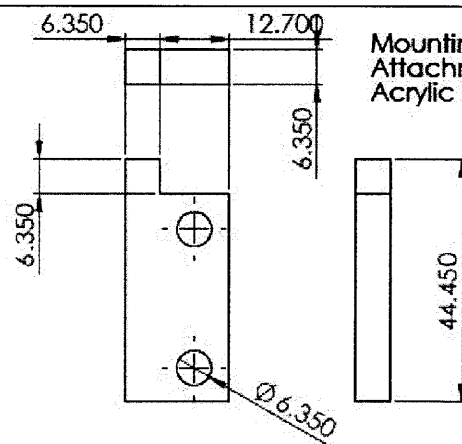
Front/Back Piece - Acrylic  
38.100



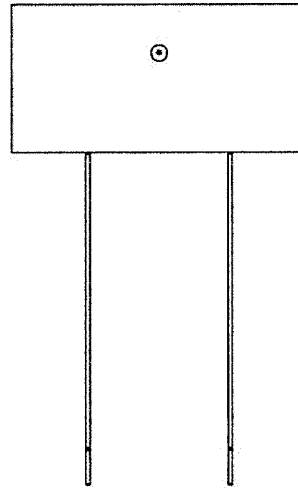
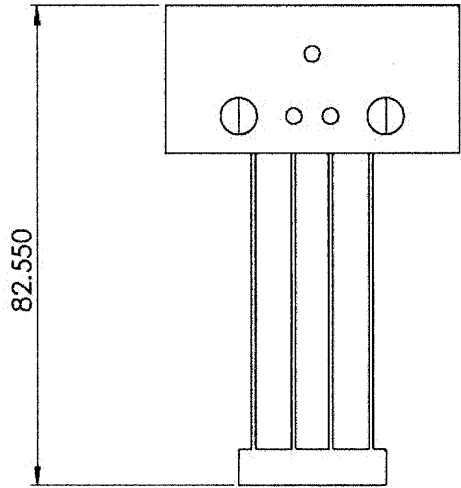
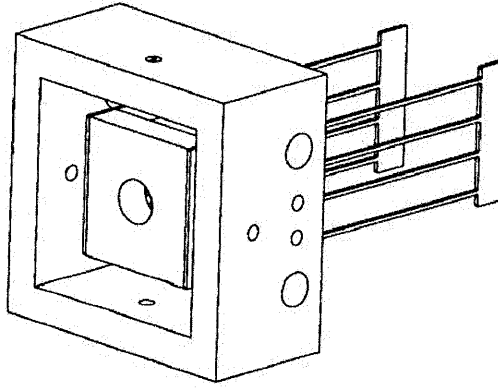
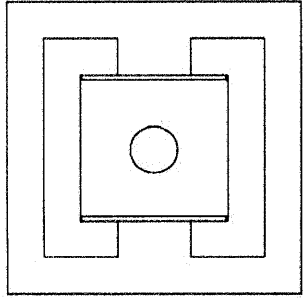
Flexing Piece - 1095 Spring Steel



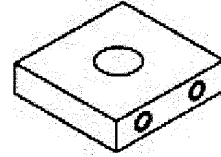
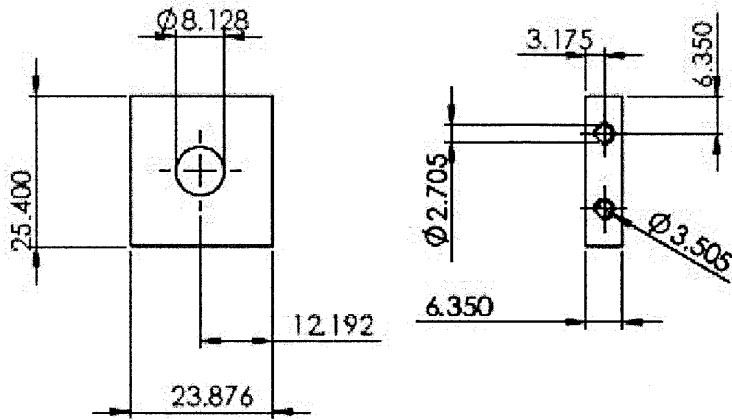
Mounting Attachment - Acrylic



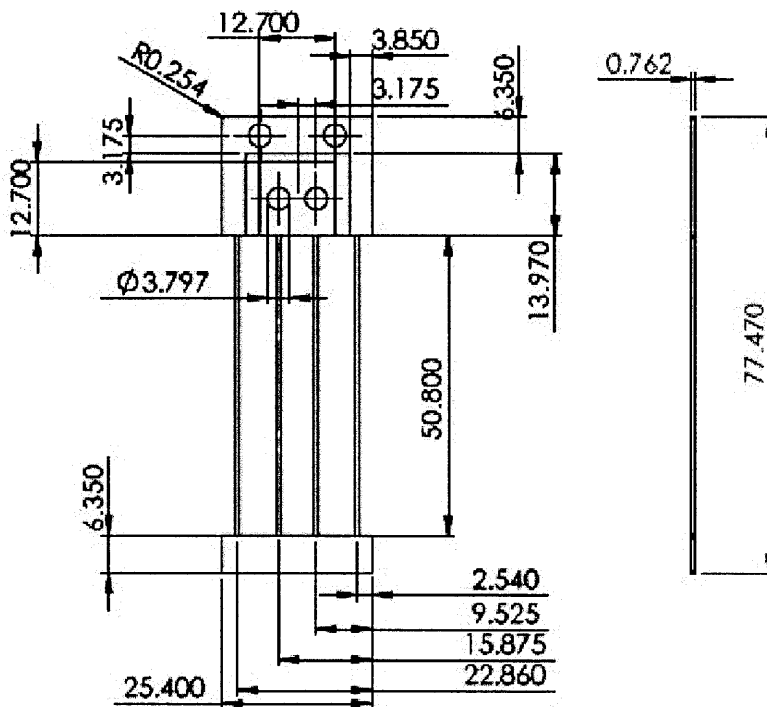
PSD Flexure Stand



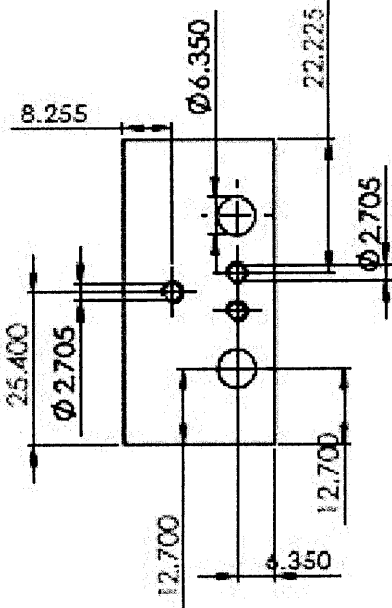
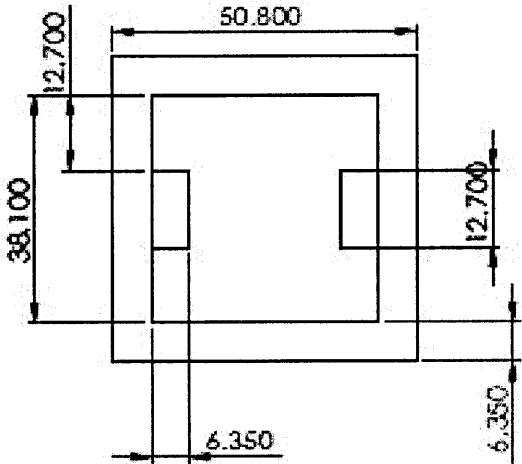
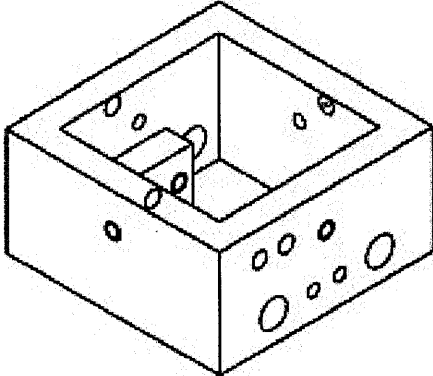
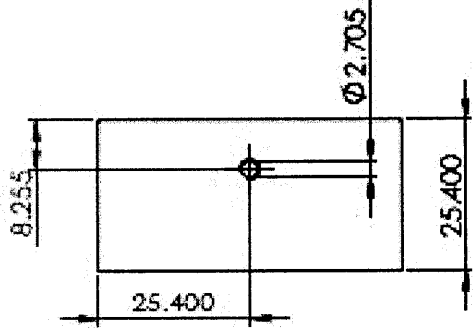
PSD Stand Stage - 6061 T6 Aluminum



PSD Stand Flexure - 6061 T6 Aluminum



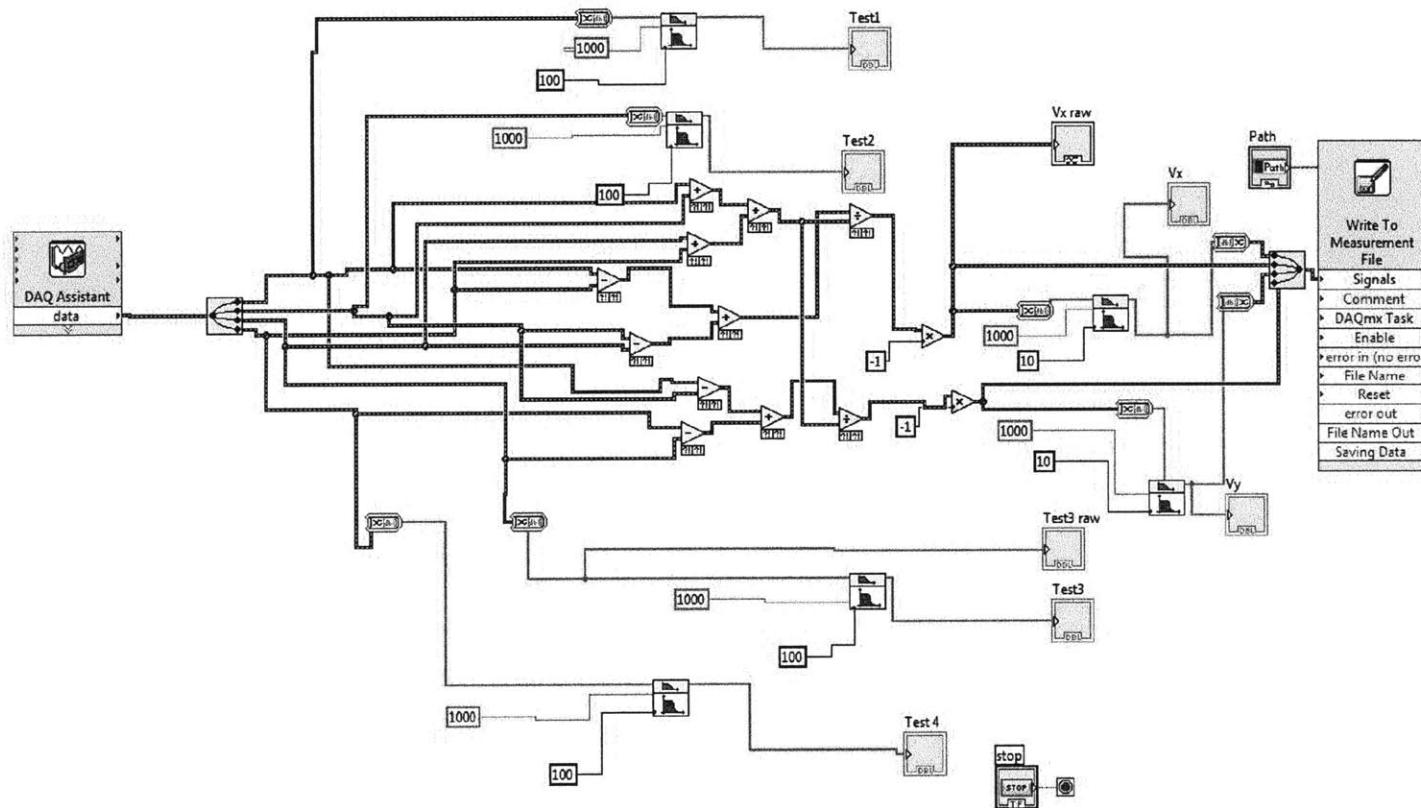
PSD Flexure Stand Base - 6061 T6 Aluminum



### **Appendix C: LabVIEW Code**

The following is an image capture of the LabVIEW block diagram constructed for the intake and digital measurement of the system. This code intakes four digital signals from the NI 9215 DAQ device and outputs a real time graph of the data passed through a noise filter for each signal.

The code also sums and normalizes these voltages to output  $V_x$  and  $V_y$  to their own noise-filtered graphs, and exports these two signals to .lvm files, which can then be imported into MATLAB as discussed above.







## 7. References

- [1] R. King, Massachusetts Institute of Technology, "Design of a Novel Six-Axis Metrology System for Meso-Scale Nanopositioners," 2009.
- [2] M.J Telleria., M.L Culpepper, Massachusetts Institute of Technology, "Understanding the drivers for the development of design rules for the synthesis of cylindrical flexures," 2012.
- [3] <<http://www2.bioch.ox.ac.uk/~oubsu/ebjknight/q4d.html>>
- [4] <<http://www.fairchildsemi.com/ds/LM/LM317.pdf>>
- [5] <[http://en.wikipedia.org/wiki/Operational\\_amplifier](http://en.wikipedia.org/wiki/Operational_amplifier)>
- [6] <<http://www.ti.com/lit/ds/symlink/lm324-n.pdf>>
- [7] <<http://www.mathworks.com/matlabcentral/fileexchange/19913>>
- [8] B. Trease, Compliant System Design Laboratory, University of Michigan, "Flexures Lecture Summary," 2004.
- [9]<<http://www.matweb.com/search/DataSheet.aspx?MatGUID=1b8c06d0ca7c456694c7777d9e10be5b>>
- [10] Craig, Roy R, and Timothy A. Philpot. *Mechanics of Materials*. New York: John Wiley, 2000. Print.
- [11]<<http://www.matweb.com/search/DataSheet.aspx?MatGUID=21bc72229925455db41e3cea6bb7625a&ckck=1>>
- [12] <<http://media.digikey.com/pdf/Data%20Sheets/US%20Lasers%20PDFs/M6505I.pdf>>
- [13] <[http://www.pacific-sensor.com/pdf\\_quadrant/QP5.8-6-TO5.pdf](http://www.pacific-sensor.com/pdf_quadrant/QP5.8-6-TO5.pdf)>